Architecture for an Ultrasound Advanced Open Platform With an Arbitrary Number of Independent Channels

Daniele Mazierli , *Student Member, IEEE*, Alessandro Ramalli , *Senior Member, IEEE*, Enrico Boni , *Member, IEEE*, Francesco Guidi , *Member, IEEE*, and Piero Tortoli , *Fellow, IEEE*

Abstract—Ultrasound open platforms are programmable and flexible tools for the development and test of novel methods. In most cases, they embed the electronics for the independent control of (maximum) 256 probe elements. However, a higher number of channels is needed for the control of 2-D array probes. This paper presents a system architecture that, through the hardware and software synchronization of multiple ULA-OP 256 scanners, may implement advanced open platforms with an arbitrary number of channels. The proposed solution needs a single personal computer, maintains real-time features, and preserves portability. A prototype demonstrator, composed of two ULA-OP 256 scanners connected to 512 elements of a matrix array, was implemented and tested according to different channel configurations. Experiments performed under MATLAB control confirmed that by doubling the number of elements (from 256 to 512) the signal-to-noise and contrast ratios improve by 9 dB and 3 dB, respectively. Furthermore, as a full 512-channel scanner, the demonstrator can produce real-time B-mode images at 18 Hz, high enough for probe positioning during acquisitions. Also, the demonstrator permitted the implementation of a new high frame rate, bi-plane, triplex modality. All probe elements are excited to simultaneously produce two planar, perpendicular diverging waves. Each scanner independently processes the echoes received by the 256 connected elements to beamform 1300 frames per second. For each insonified plane, good quality morphological (B-mode), qualitative (color flow-), and quantitative (spectral-) Doppler images are finally shown in real-time by a dedicated interface.

Index Terms—3-D beamforming, high frame rate imaging, matrix array, multi-channel, open scanner, sparse array, synchronization, ultrasound.

I. INTRODUCTION

MEDICAL ultrasound (US) echographic systems typically consist of a multi-channel electronic scanner and an array of transducers. In research contexts, full and independent control of all the array elements is fundamental to provide maximum flexibility to the development and experimental test of original novel methods. This is today possible thanks to the so-called open scanners [1] that have fueled innovation in the field of US medical imaging.

Most advanced open scanners embed the electronics for the generation of the transmission (TX) signals and the reception (RX), acquisition, and processing of the echo signals. They typically provide up to 256 independent channels, which are sufficient for flexibly controlling 1-D linear, convex, or phased arrays. These arrays were used to introduce groundbreaking methods such as high-frame-rate B-mode [2] and Doppler [3], [4] imaging, and also to promote 3-D imaging by mechanical scans, although at very low volume rates [5]–[9].

Definitely, fast electronic scans of the volumes of interest need to be based on 2-D matrix arrays [10]–[14]. Unfortunately, 2-D arrays involve higher numbers (up to thousands) of transducer elements, which makes challenging the electrical interconnections, the signal routing, and the channel count of the companion open scanner. This problem can be tackled by the development of application-specific integrated circuits (ASICs), directly embedded in the probe, to reduce the channel count through the so-called micro-beamforming [15]–[18], or by suitably designing sparse arrays [19]–[23] to have as many elements as the scanner channels. However, the former solution unavoidably limits the flexibility and, thus, the possible development of novel imaging modalities, while sparse arrays, although achieving reasonably good resolution and contrast [24], penalize the sensitivity and the signal-to-noise ratio (SNR) [25]–[28]. Hence, there is an urgent need for research systems with high numbers of independent channels for the development and test of novel imaging methods, possibly without a tradeoff on image quality, flexibility, raw data accessibility, and real-time performance.

Only a few research systems with more than 256 channels have been so far presented. Two 256-channel open scanners of the ULA-OP 256 [29] family were used together for applications such as tri-plane echocardiography [24] and super-resolution 3-D imaging [26]. 512 elements were controlled but, since the two scanners were connected to independent dedicated personal computers (PCs), the user had to: manually control the computers, separately run the two software interfaces, and

merge, in post-processing, the related acquisitions. According to this procedure, the system synchronization turned out to be quite complex, and not extendable to more than two scanners. Furthermore, the beamforming of all 512 channels could not be realized in real-time.

The SARUS scanner [30] (Technical University of Denmark), can control up to 1024 transducer elements of a matrix probe and simultaneously receive on all channels. Housed in a double rack of size $120 \times 200 \times 60$ cm, it is a complex system whose main specification was the high computational power, without any constraint in terms of portability and cost. It was shown effective to acquire synthetic aperture data that were post-processed for 3-D flow imaging by using either 2-D [31] or row-column addressed arrays [32]. An alternative approach was followed by the Langevin Institute in Paris and the University of Lyon for their 1024-channel systems: these were obtained by multiplexing 4 Aixplorer [33] and parallelizing 4 Verasonics [34] open scanners, respectively. In both cases, each scanner was connected to a companion PC and to a group of 256 probe elements, proposing a cumbersome configuration characterized by extended data acquisition capability but limited real-time processing performance and portability. These systems were exploited for retrospective 3-D ultrafast imaging [35], [36] and testing of optimized sparse array [25], [37]. Finally, the software-based platform us4R^{TM} [38], [39] provides up to 1024 independent channels in TX, but the number of RX channels is currently limited to 256.

This paper presents a novel system architecture that, through the hardware and software synchronization of multiple ULA-OP 256 scanners, may implement a research platform with an arbitrary number of independent channels. The proposed solution requires the use of a single PC, maintains real-time features, and (to some extent) preserves portability. The effectiveness of this approach is shown by a prototype demonstrator consisting of two synchronized ULA-OP 256. These can work as a single 512-channel scanner or according to a variety of configurations, in which they act as scanners that synchronously, but independently, manage two probes or two sub-apertures of the same 2-D probe.

The paper is organized as follows: Section II provides details of the hardware and software developed to synchronize the TX/RX of multiple ULA-OP 256 scanners. The main characteristics of a 512-channel demonstrator, including a 512-element 2-D array probe, are described in Section III. The next Section reports on the experiments to evaluate the real-time processing power and the performance in terms of synchronization, image quality, and frame rate. The results are finally discussed in Section V.

II. MULTIPLE SCANNERS SYNCHRONIZATION

A. Basic Configuration of ULA-OP 256

The ULA-OP 256 [29] is an ultrasound open platform designed by the Microelectronic Systems Design Lab (MSDLab) of the University of Florence (Italy). This hardware-based platform [1] can independently control up to 256 transducers and is highly flexible in both TX and RX. This result is obtained thanks
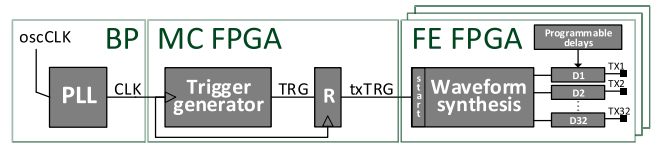

Fig. 1   TX signals generation. The txTRG signal, synchronous with CLK, initializes the generation of the 32 TX signals in each of the 8 FE boards. The actual delay of each signal start (Di) can be arbitrarily programmed. The same CLK and txTRG signals are also used to synchronize all RX operations.

to a modular architecture, in which 8 identical Front-End (FE) boards control 32 TX/RX channels each. The FE boards are interconnected through a high-speed serial rapid input-output (SRIO) link running on the Backplane (BP), which also hosts a Master Control (MC) board that oversees all FE operations. The MC board is connected through a USB 3.0 link to a host PC on which a dedicated (C++) software instance runs. The software, which is supplied together with the scanner, initializes the hardware upon startup, runs the application-specific processing modules, and displays the results in a user-friendly real-time interface.

All TX/RX operations of the scanner are controlled by an internal 78.125 MHz system clock (CLK). As shown in Fig. 1, CLK is generated on the BP by a programmable low-jitter (<500 fs) phase-locked-loop (PLL, AD9522-4, Analog Devices), fed by the oscillator clock (oscCLK). CLK is then forwarded to the MC field programmable gate array (FPGA, Cyclone V SoC, Altera, San Jose, CA, USA), where a programmable counter generates an internal trigger (TRG). The latter one is sampled by an internal register (R) to produce the synchronous transmission trigger (txTRG), which is distributed to all the FE boards to periodically start, at a rate equal to the pulse repetition frequency (PRF), the TX events. For each active channel, the analog TX signal is obtained by low-pass filtering a corresponding 625 MHz sigma-delta bitstream [40] produced by the FE FPGA (ARRIA V GX, Altera, San Jose, CA, USA). The actual start of each TX signal is initialized by the txTRG signal, but the user can also program arbitrary offset delays (as needed for TX beamforming).

The same CLK and txTRG signals are also used to synchronize all RX operations. The echo signals are digitized at 78.125 MHz with 12-bit resolution, beamformed by the same FE FPGAs and further processed by embedded digital signal processors (DSPs, 320C6678, Texas Instruments, Austin, TX, USA), which allow the real-time implementation of quadrature demodulation and computationally demanding processing techniques [24], [29], [41]. Moreover, the ULA-OP 256 scanner permits storing and downloading up to 80 GB of raw, post-beamforming, or demodulated data.

B. Hardware and Software Synchronization of Multiple ULA-OP 256

The overall number of channels can be extended by using multiple ULA-OP 256 scanners, provided they work synchronously, i.e., with fully synchronous CLK and TRG signals. To this
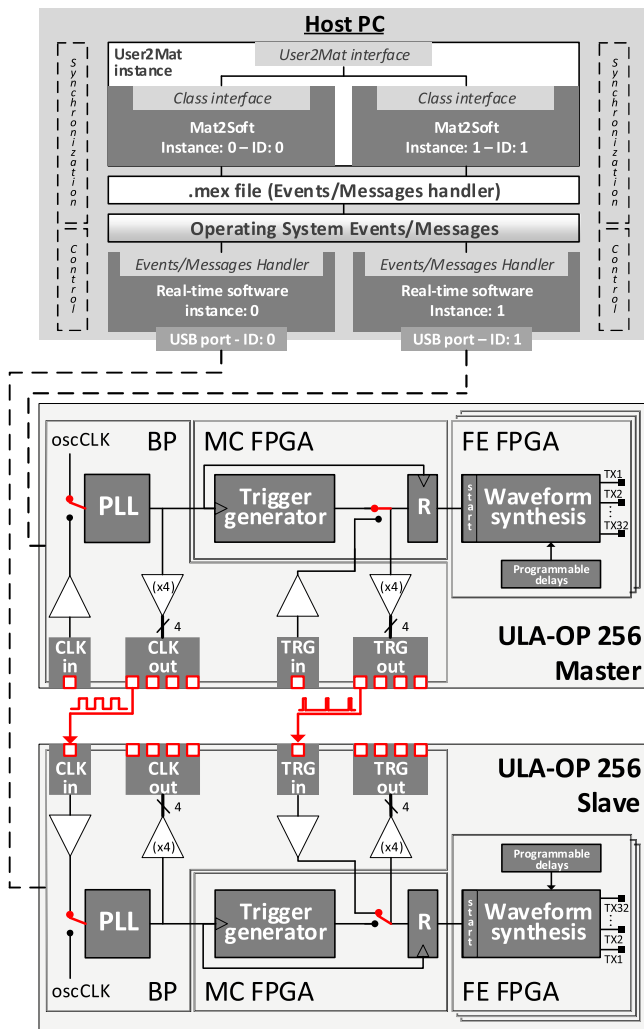
Fig. 2 Block diagram of a 512-channel system showing the hardware interconnections and software communications. Two software layers (control, synchronization) run on the host PC at the same time. The communication between layers exploits the operating system's events and messages, while the communication with the user exploits the User2Mat.m class interface. The class Mat2Soft.m is dedicated to the synchronization of the scanners.

Master txTRG, although possibly delayed by one or more (N) CLK periods of duration 12.8 ns. The number of periods, N, is related to the delay between the Master TRG and the Slave TRG signals, which may be assumed equal to the measurable delay between the signals on the TRGout connectors (see Fig. 2). Finally, the delay, $N \times 12.8$ ns, of the Slave txTRG(s), can be compensated by programming, in the Master FE FPGAs, a corresponding offset delay for all TX signals. It is noteworthy that the calibration must be conducted only once, and no re-calibration is needed unless the CLK and TRG connection cables are changed. Afterwards, CLK and TRG delays are automatically compensated at each startup of the system.

Since 4 CLKout and 4 TRGout connectors are available, up to 4 Slaves could be connected to one Master. Fig. 2 shows the hardware interconnections and software communications when one Master is connected to one Slave, but the block diagram can be extended for more Slave scanners.

The host PC is connected to any ULA-OP 256 through a USB 3.0 link, which is uniquely identified by the identification number (ID) of the USB port. The original ULA-OP 256 real-time software was modified to allow running multiple instances and establishing a point-to-point connection with a specific scanner by the USB ID. Since the multiple instances of the real-time software were not able to communicate among them, the software architecture was extended with an additional software layer (the synchronization layer, Fig. 2) to synchronize and manage an arbitrary number of ULA-OP 256 scanners.

The synchronization layer consists of two MATLAB (The MathWorks, Natick, MA) classes, interfacing the dedicated software (Mat2Soft.m) and the user (User2Mat.m). Through these classes, which are included in the supplied software bundle, the user can power on/off the scanners, configure the TX/RX modes, run the real-time software instances, freeze/unfreeze the acquisition, change processing parameters, and download the acquired data, without caring about the synchronization, which is transparently managed by the classes.

The user interfaces with only the MATLAB environment through a script that instantiates one single object of User2Mat type, specifying the number of connected scanners. Then, the whole system can be controlled through the specific methods offered by the object. The User2Mat class constructor automatically instantiates, for each scanner, a Mat2Soft object, which is in charge of managing the communication between the MATLAB environment and the software control layer (Fig. 2), implemented by the C++ real-time interface. The communication exploits the operating system's events and messages, which are coded and addressed with the ID of the USB port to which the specific ULA-OP 256 is connected to and are handled by a purposely developed MATLAB executable file (.mex) interface.

Thanks to this architecture, the system can be controlled in two different ways: the echo data received by each synchronized scanner can be independently processed and displayed through the related real-time interfaces and, still in real-time, they can be (possibly) merged, processed, and displayed through the MATLAB interface/environment, all without interfering with the acquisition capabilities.

aim, the ULA-OP 256 was modified to support a multi-scanner "Master-Slave" configuration.

In each scanner, both the CLK and TRG signals were buffered toward corresponding output connectors, hereinafter referred to as CLKout and TRGout, respectively (see Fig. 2, bottom panels). Such connectors were wired from the Master scanner to the CLKin and TRGin inputs of one (or multiple) scanner(s), programmed to act in "Slave" mode.

In the Slave scanner(s), the CLKin and TRGin signals were buffered toward the internal logic circuits, so that:

1) CLKin fed the BP PLL to produce, with programmable phase delay, the CLK signal;
2) TRGin fed the R register within the MC FPGA, to generate a synchronous txTRG signal.

In this way, each Slave PLL can be programmed to achieve a zero-delay between the CLK signals of the scanners. Consequently, all the Slave txTRG signals result synchronous with the
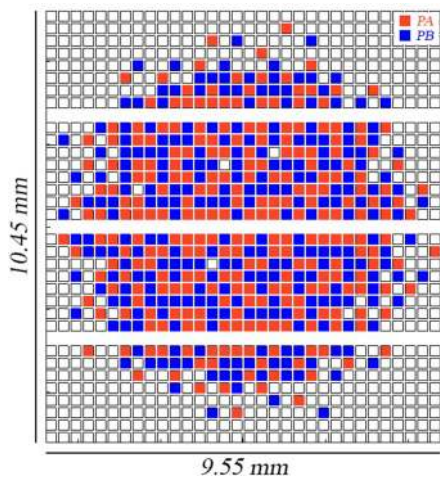
Fig. 3 The 512-channel demonstrator.

Fig. 4 Layout of PA (red) and PB (blue) element subgroups. PA and PB can be synchronously controlled by two ULA-OP 256 both as a 512-element dense array, in TX, and as independent 256-element spiral arrays, in RX. Note: the three horizontal missing lines are due to construction/wiring constraints.

III. 512-CHANNEL DEMONSTRATOR

The effectiveness of the proposed architecture was assessed by building a 512-channel system (Fig. 3) based on two ULA-OP 256 scanners connected to a 512-element prototype 2-D probe. First, the two scanner CLKs were synchronized. Then, the phase delay between the Master txTRG and the Slave txTRG was compensated. The performance of the system was evaluated considering different TX/RX configurations of active elements/channels. B-mode imaging was used to evaluate the image contrast and achievable frame rate, while multigate spectral Doppler (MSD) [42], [43] was adopted to estimate the SNR. Finally, the "expanded" computational power of the system was demonstrated by an experiment in which the two scanners, connected to two subgroups of elements of the same probe, independently perform demanding processing tasks in real-time.

A. 2-D Probe

In this work, a special version of the 1024-element Vermon 2-D matrix array probe (Vermon S.A., Tours, France) [26] was adopted. The probe elements (3.7 MHz center frequency, 70% bandwidth, 300 μm pitch) are organized in 32 (x-axis) columns by 35 (y-axis) rows, with every ninth row on the y-direction not connected. Two different probe configurations (hereinafter referred to as PA and PB) were obtained by choosing two sets of 256 elements each (Fig. 4) and wiring them to distinct connectors [24]. The PA elements were selected trying to match, as much as possible, the ideal positions of the seeds in a Tukey-tapered spiral array [23]. Among the remaining 768 elements, the PB elements were selected by matching the seeds' position of a second Tukey-tapered spiral array, which resulted rotated compared to PA. In this way, by connecting the two arrays to two ULA-OP 256, both the sparse subsets of elements could be driven either independently or synchronously (PA+PB). In the latter case, a denser probe with Tukey density tapering was obtained.

B. Probe/System Configurations

The Slave scanner was connected to the elements of PA, while the Master scanner was connected to PB's elements. Five distinct system configurations were considered:

1) 256TX-RX (PB): only the 256 elements of PB were simultaneously used in both TX and RX.
2) 256TX-RX (PA): only the 256 elements of PA were simultaneously used in both TX and RX.
3) 512TX–256RX (PB): all 512 elements were simultaneously excited in TX, but only the PB's elements were used in RX by the Master.
4) 512TX–256RX (PA): all 512 elements were simultaneously excited in TX, but only the PA's elements were used in RX by the Slave.
5) 512TX-RX: all 512 elements (PA+PB) and channels were simultaneously used in both TX and RX.

The first two configurations permitted evaluating the imaging performance achievable when a single scanner was used together with the 256 elements of either PA or PB. Configurations 3 and 4 allowed estimating the improvements achievable by doubling the number of TX elements. Finally, the last configuration enabled the testing of the performance of:

- a system working as a 512-channel scanner that operates through the MATLAB environment;
- a system in which two scanners simultaneously excite 512 probe elements, but independently process, in real-time, the echoes received by two subgroups of 256 elements each.

C. Imaging Modes

For each of the above configurations, two different imaging modes were implemented:

- B-mode: 3-cycle, Hamming-tapered sinusoidal bursts at 3.7 MHz were used to transmit, at 5 kHz PRF, ultrasound beams focused at 30 mm along 100 different directions to cover an imaging sector of 80°.

- MSD-mode: 5-cycle, Hamming-tapered sinusoidal bursts at 3.7 MHz were used to transmit, at 1.5 kHz PRF, ultrasound beams focused at 30 mm along the direction coincident with the probe axis.

For both modes, the echo signals, received from different distances (also referred to as depths) along the line of interest, were apodized and 3-D dynamically focused (i.e., beamformed) by the FE FPGAs. Then, the data were demodulated and low-pass filtered by the DSPs onboard each ULA-OP 256 scanner. For the B-mode, the data were also log-compressed and, finally, scan converted and displayed as a greyscale image. For the MSD-mode, the data for each depth were weighted with 128-point Hann's windows in the slow-time and then converted to frequency by a fast Fourier transform (FFT). Clutter filtering, designed as a frequency domain mask, removed the spectral components close to zero frequency. The log-compressed spectral intensities were color-coded to form images in which the vertical axis corresponded to the depth, while the horizontal axis to the Doppler shift.

To assess B- and MSD-mode image quality, the baseband data obtained for each configuration were saved on the host PC and post-processed in MATLAB with a script that replicates the above real-time processing steps implemented on the ULA-OP 256.

Finally, a novel real-time (triplex bi-plane) high frame rate (HFR) modality, needing a computational power higher than that provided by a single scanner, was tested. The goal was displaying in real-time, for two different (perpendicular) planes, morphological (B-mode), qualitative (color flow imaging, CFI) and quantitative (MSD) flow information with high time resolution. Specifically, the (PA+PB) probe transmitted two simultaneous, planar diverging waves [24], [44] with rotational angles of $0°$ and $90°$. For each TX event at 1300 Hz PRF, the Master and Slave scanners independently processed the echo data received by the PB and PA elements, respectively, to image the $60°$-wide insonified planes (bi-plane imaging). For each scan plane, 100 lines were parallel beamformed, demodulated, and filtered. Then, still in real-time, the data of each frame were processed according to three different imaging modes: HFR B-mode, HFR CFI [41], and MSD. In particular, CFI processing involves, for each point of the image: (1) a continuous-time, fourth-order, infinite impulse response high-pass filtering, to separate the blood signal from clutter; (2) the computation of the signal power, lag-one autocorrelation [45] and standard deviation on 32 complex samples; (3) the application of spatio-temporal low-pass filters and the extraction of the phase of the autocorrelation function.

IV. EXPERIMENTS

A. Scanners Synchronization

The Master and Slave CLKout and TRGout signals were connected, through coaxial cables of equal length, to the Keysight DSOX3022T digital oscilloscope (Keysight Technologies Inc., Santa Rosa, CA).

The synchronization of the two scanners was achieved in two steps:

1) The phase of the Slave scanner's PLL was adjusted until the two CLKout signals looked fully overlapped on the oscilloscope.
2) The phase delay between the two TRGout signals was measured equal to 15.6 ns. This was consistent with the range of values, [8.4, 16.2] ns, expected considering the variability of propagation delays within the synchronization circuits as well as the length of the connecting cables. The measured delay was longer than one CLK period (12.8 ns) but shorter than two periods (25.6 ns): accordingly (see Section II.B), the delay between the corresponding txTRG signals at the register output (Fig. 1), was thus considered equal to one CLK period. This (Slave) txTRG delay was finally compensated by delaying the start of all TX signals in the Master scanner with an offset of 12.8 ns.

The effectiveness of the overall calibration was verified by acquiring onto the oscilloscope the TX signals present at the outputs of the same channel in the Master and the Slave scanner, respectively. The acquired digital signals were passband filtered, cross-correlated, and the delay of the cross-correlation peak was assumed as the uncompensated phase delay between the txTRG signals. To better estimate such delay, narrow and peaked cross-correlation waveforms were obtained by simultaneously transmitting, from all 512 channels, 6-μs-long, Tukey-tapered chirps having a 10 MHz bandwidth around 6 MHz.

Fig. 5a shows the initial part of the TX chirps signals acquired on Slave (red) and Master scanners, before (black) and after (blue) the compensation. Fig. 5b shows the normalized cross-correlation between Master and Slave TX signals, before (black) and after (blue) the compensation. The good alignment between the red and the blue TX signals, as well as the lower phase delay assessed from the compensated correlation, confirms the effectiveness of the compensation procedure. For this specific case, the measured phase delays before and after compensation were 13.2 ns and 0.4 ns, respectively, while the phase delay measured across 15 randomly selected channels was 0.2 ± 0.7 ns after the compensation. Such phase delays (<1 ns) correspond, at the maximum ULA-OP 256 TX frequency (20 MHz), to less than 1/50 of the waveform period (50 ns), and can thus be considered negligible.

B. B-mode Imaging Test

1) B-mode Contrast: B-mode baseband data, related to 20 consecutive frames, were post-processed and used to compare, in MATLAB, the contrast achievable by the different configurations. These tests were based on the commercial tissue-mimicking phantom 404GS LE (Gammex Inc., Middleton, WI), which includes wires, hyperechoic, and anechoic cysts.

Fig. 6 shows two B-mode sample images obtained with the 512TX-RX and 256TX-RX configurations. Even if the two images look similar, the contrast is slightly improved when two synchronized scanners are used. To verify this, two different regions, both at the focal depth, were identified in the background (S_{ROI}) and within the anechoic cyst (CN_{ROI}) [46], respectively. The contrast ratio (CR) was calculated as the ratio between the mean echo intensities in S_{ROI} an CN_{ROI}.
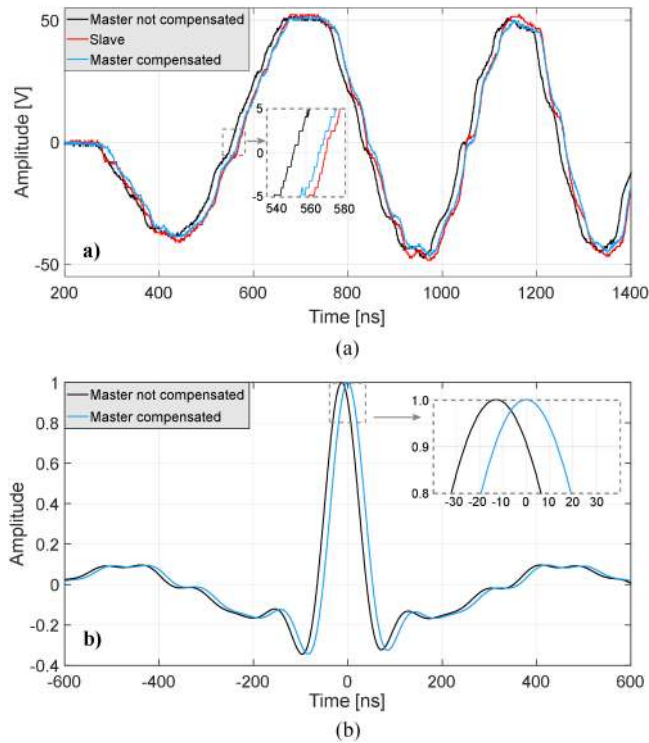
Fig. 5   (a) Sample TX signals recorded at the same channel output of the Master and Slave scanners. The red signal is the TX waveform generated by the Slave scanner, while the black and blue signals are those generated by the Master before and after the synchronization, respectively; (b) correlation functions between Master and Slave TX signals. The black and blue signal were obtained before and after the Master compensation, respectively. To make the plot readable, only short time intervals of the chirp (a) and of the normalized cross-correlation (b) signals are shown, and further magnifications are highlighted in the dashed rectangle.
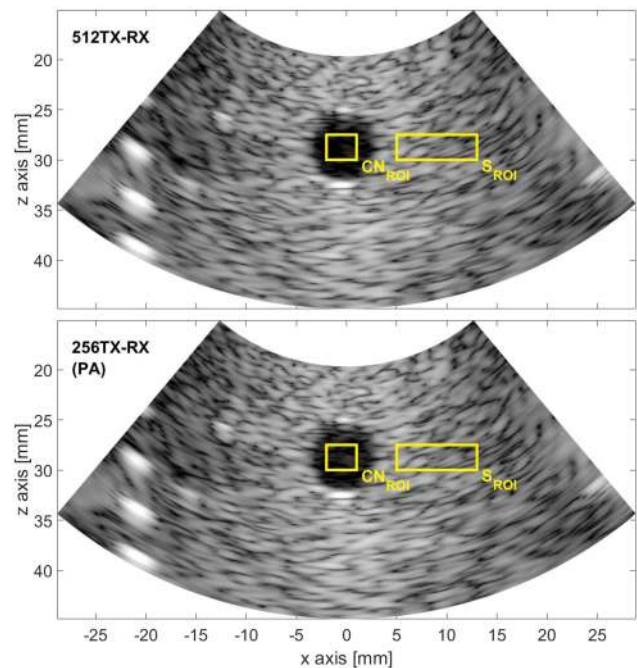

Fig. 6   B-mode images obtained with the 512TX-RX (top) and the 256TX-RX (PA) configuration (bottom), respectively. The regions indicated with CN_{ROI} and S_{ROI} were selected at the 30 mm focal depth, in the anechoic cyst and in the background, respectively.

TABLE I
- CR AND SNR VALUES* OF TESTED CONFIGURATIONS.

	256TX-RX (PB)	256TX-RX (PA)	512TX-256RX (PB)	512TX-256RX (PA)	512TX-RX (PA+PB)
CR [dB]	-1.8	-3.2	-0.1	-0.5	0.0 (22.1)
SNR [dB]	-7.4	-9.4	-3.0	-3.1	0.0 (38.9)

*All values are normalized to the value obtained with the 512TX-RX configuration, here assumed as reference. The absolute values obtained for the 512TX-RX configuration are reported in brackets.

The first line of TABLE I reports the CR differences among all tested configurations. The measured CR values appear to mainly depend on the number of transmitting channels: higher contrast values are obtained with 512TX, while the number of receiving channels has minimal impact.

2) B-mode Frame Rate: B-mode imaging was also used to assess the maximum achievable frame rates, at different PRF values, when interfacing the system through the MATLAB environment. To create one frame, four macro-operations were involved: (1) scan and formation of the 100 imaging lines, (2) transfer of each demodulated frame (400 kB), composed of 512 depths × 100 lines, onto the hard drive of the host PC, (3) reading of such data on MATLAB, (4) offline elaboration, log-compression, and display. To speed up the frame rate, some of these operations were performed in parallel. Specifically, while the system was acquiring and downloading one frame, the MATLAB process read and processed the previously acquired frame. The maximum achievable frame rate was thus limited by the most time-consuming of the two operations. The testbench for frame rate evaluation included a host PC embedding an Intel core GHz processor, 64 GB of DDR4-2132MHz random access memory (RAM), a Samsung 512 GB PCIe 3.0 x4 solid-state disk (SSD) EVO, and a Seagate 2TB 7200 rpm SATA-III magnetic drive (MD).

In a MATLAB script, the time interval between two consecutive B-mode frames was measured and 50 measurements were averaged to estimate the real-time frame rate. Fig. 7 illustrates the frame rate trends obtained for all tested configurations. The results indicate that the real-time performance changes with the host PC technology (hard drive type being the most important item) and with PRF. Fig. 7 shows that, as expected, at any PRF value the use of the SSD, which provides shorter read and write times, leads to better frame rates compared to the use of the MD. Also, the frame rate is higher when the data acquired from only one scanner, as in the 256TX-RX configuration, must be written, read, and processed. Overall, when using a fast SSD, a real-time frame rate of almost 18 Hz and 24 Hz could be obtained in B-mode imaging with 512TX-RX and 256TX-RX configurations, respectively. It is worth noting that, even if the
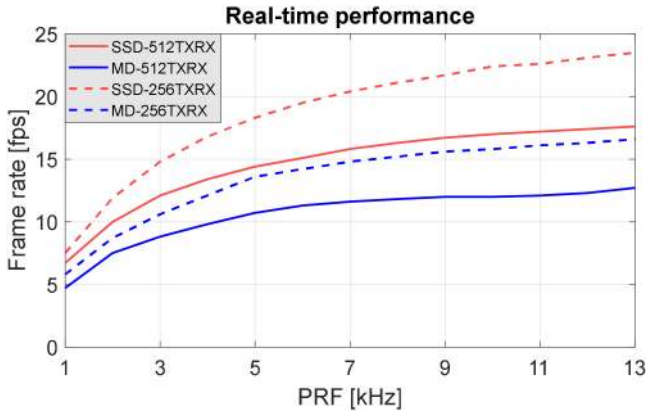
Fig. 7   Frame rate trends for different PRF values, hard drive technologies, and channel configurations. The blue lines were obtained using the magnetic disk (MD), while the red lines using the solid-state drive (SSD).

frame rate is expected to be linearly related to the PRF, the trends in Fig. 7 are asymptotic. Indeed, although the PRF was increased, the hard drive access time became dominant and, beyond 13 kHz, further PRF increases did not imply significant increases in the frame rate.

C. MSD Imaging Test

An experimental setup was assembled, in which a blood-mimicking fluid flew in a cylindrical Rilsan pipe immersed in a water tank. The fluid was composed of a mix of 2 g of 10 μm polyamide spherical particles (Orgasol, Arkema Inc., Philadelphia, PA) and 2 liters of demineralized water, suitably stirred to obtain a homogeneous suspension. According to [47], such a particle concentration ensures backscattering features similar to those of blood. The fluid was driven at a steady rate by a peristaltic pump (Watson-Marlow, Falmouth, U.K.).

The MSD frames in Fig. 8 clearly show the expected parabolic flow profile for all tested configurations. The SNR was assessed for all configurations as follows. As shown in the right panel, the region including the flow spectral contributions, labeled as S_{ROI}, was delimited by the -6 dB isolines. The noise region (N_{ROI}) was selected in the upper portion of the image and included $n_N = 60$ depths where the flow was not present. The SNR was estimated as:

$$SNR = 10\log_{10}\left(\frac{S}{N}\,\frac{n_N}{n_S}\right) \qquad (1)$$

where S and N are the overall Doppler and noise signals power measured in S_{ROI} and N_{ROI}, respectively, while n_S is the number of depths included in the S_{ROI}.

The quantitative results reported in TABLE I highlight an improvement of about 6 dB when the number of TX elements is doubled, while further 3 dB improvements are obtained doubling the number of RX elements.

D. Real-time, high-frame-rate, Bi-Plane Triplex Mode

1) Acoustic Beam Measurements: One-way fields were acquired for the triplex bi-plane mode introduced in Section

III.C. The emitted pressure was measured by an HGL008 hydrophone (Onda Corporation, Sunnyvale, CA, USA), connected to a low noise amplifier (Onda, mod. AH-2010) followed by a 12-bit analog-to-digital converter working at 125 MHz. The hydrophone and the probe were aligned and immersed in demineralized water. The pressure signals were acquired on a regular grid of 151 × 151 points covering a region of 40 mm × 40 mm. Such region was placed on three planes: x-z, y-z, and x-y (at z = 20 mm). For each hydrophone position, the peak pressure values were extracted and log-compressed to create the beamplots shown in Fig. 9.

As expected, the orthogonal diverging waves generated a crossed pressure field (Fig. 9b), with unavoidable lateral lobes due to the unfocused transmission. On the x-y plane, the peak pressure value was located at the intersection of the two diverging waves, coincident with the probe axis. Particularly, Fig. 9c and Fig. 9d confirmed that the peak pressure value, P_{max}, was measured at about 20 mm far from the probe surface.

2) Real-time Experiment: The real-time performance of the novel mode was tested on a commercial flow phantom (Ats Laboratories Inc, Bridgeport, CT). A peristaltic pump (model 120 U, Watson-Marlow Limited, Falmouth, U.K.) pushed a commercial 069-DTF blood-mimicking fluid (Cirs Inc., Norfolk, VA) into the 8-mm diameter cylindrical pipe. The flow was further controlled by a solenoid valve, driven by a pulse-width modulated signal at 1 Hz and 60% duty cycle.

Fig. 10 shows a screenshot of the graphical user interfaces that display, in real-time, the results of the triplex processing. The availability of such a real-time display allowed aligning the probe and the investigated vessel so that the two scan planes intercepted cross- and longitudinal-sections of the pipe. The left window was produced by the Master scanner connected to PB, while the right window was produced by the Slave scanner connected to PA. The B-mode and CFI data were superimposed in panels M_0 and S_0, to provide both morphological and flow qualitative information. On each of these panels, the yellow line indicates which of the 100 available beamformed lines was used to perform MSD analysis, whose results are displayed on the lateral (M_1, S_1) panels. Finally, on M_1 and S_1 panels, the horizontal white lines indicate the depths corresponding to the spectrograms shown in the bottom panels (M_2, S_2). In this setting, the system allowed obtaining, in real-time, a maximum of 1300 frames per second, which were further processed to produce sonograms, MSD, and color flow images at 40 frames per second.

The accompanying video clip shows a 15-second-long screen capture of the real-time interfaces during the experiments. The clip highlights the dynamicity of the flow: the 6-second long sonograms clearly show the periodic succession, dictated by the pump, of velocity (systolic) peaks and (diastolic) valleys; the MSD profiles highlight the parabolic shape of the flow within the tube, during systole, and the backflow close to the wall, which appears during the diastolic phase; finally, the CFI highlights the different Doppler angles obtained by sector scanning and shows a marked aliasing effect at the systolic peaks.
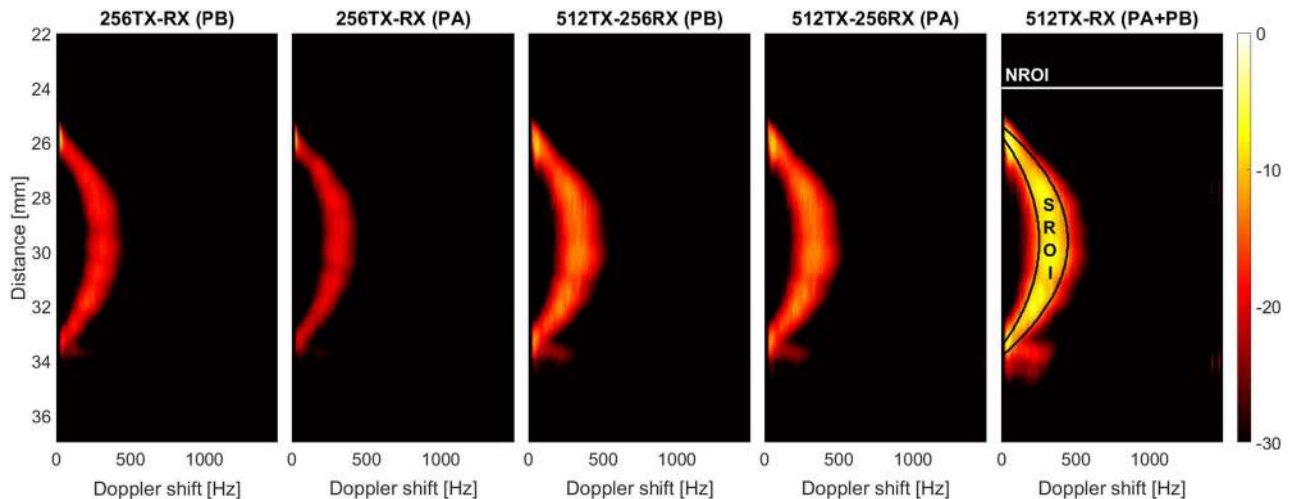
Fig. 8 Examples of MSD images obtained for all the tested configurations. The signal (S_{ROI}) and the noise (N_{ROI}) regions were automatically selected and used to calculate the SNR value, as detailed in Section III.C.
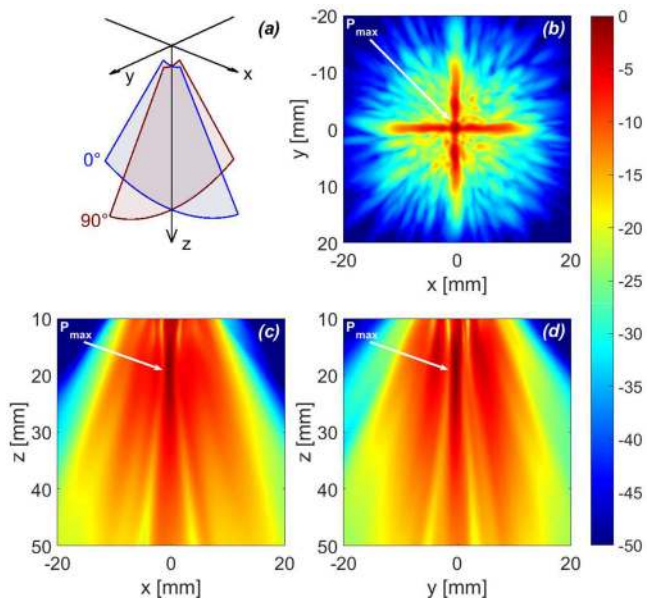

Fig. 9 Bi-plane ultrasound transmission. The reference system (a), whose origin is at the center of the probe surface, highlights the two perpendicular sectors insonified by bi-planar diverging waves. The beamplots were measured on the planes: x-y (at z = 20mm) (b), x-z (c), and y-z (d). The colorscale is in dB and normalized to the peak pressure. At 20 mm depth, the (-6dB) spatial resolution was 1.2 mm along the lateral direction and 0.8 mm along the axial direction, respectively.

V. DISCUSSION AND CONCLUSION

In this paper, the architecture of an ultrasound research system capable of supporting an arbitrary number of independent channels has been presented. Compared to the systems presented in the Introduction, the proposed solution is by far more flexible, less cumbersome, and offers effective real-time capabilities. Such an architecture is based on multiple ULA-OP 256 scanners, of which one acts as Master, providing the hardware synchronization signals (CLK and TRG) to the other (Slave) scanners.

Up to 4 Slaves can be directly connected to a single Master, for a total of 1280 channels but, in principle, this number could be further extended with a multi-level organization, by cascading up to 4 more (second level) Slaves to each (first level) Slave, thus promoted to the role of (second level) Master.

The software of the architecture was embedded into a single host PC. As shown in Fig. 2, each scanner independently communicates, through a USB 3.0 link, with a dedicated instance of the real-time software. In turn, all the instances communicate, through the operating system's events and messages, with a single MATLAB class, which has been developed to fulfill the task of synchronizing the operations of the connected scanners. A further MATLAB class was created to allow the user to friendly control such a complex ensemble of scanners as if they were a single system.

The effectiveness of the proposed solution was shown through the implementation of a 512-channel demonstrator using two synchronized ULA-OP 256 scanners connected to a 512-element 2-D prototype probe.

First, the method proposed to calibrate and compensate the CLK and TRG phase delays between the scanners was proven to be effective, with a negligible residual mismatch on the transmission waveforms due to measurement uncertainties. Then, the quality of B-mode and Doppler images provided by the proposed architecture was tested for different system configurations. As reported in TABLE I, the estimated SNR values met the theoretical expectations: when the number of TX or RX channels is doubled, a 6 dB or a 3 dB SNR gain is correspondingly entailed, with an overall SNR gain of about 9 dB when both TX and RX channels are doubled. The CR was mainly influenced by the number of transmitting elements: a denser (i.e., less sparse) element distribution produces TX beams with lower side-lobe levels, which are known to be the main source of CR degradation. When using only the elements of PB, the performance in terms of CR and SNR was slightly better (+1.4 dB and +2 dB, respectively) than that obtained using only the elements of PA. Although the two spiral configurations should ideally provide
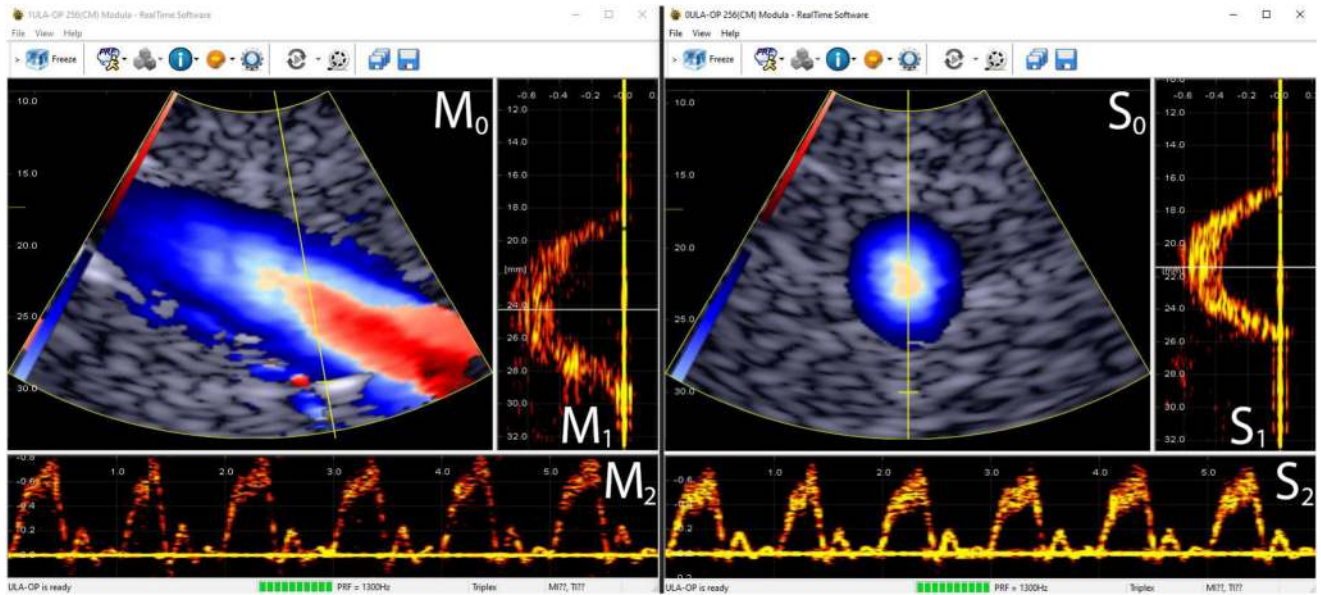
Fig. 10   Screenshot of the graphical user interfaces during the real-time test of the novel HFR triplex bi-plane real-time mode. The left window was produced by the Master, while the right one by the Slave scanner. Both windows were split in three different panels displaying B-mode and CFI images (M_0,S_0), MSD images (M_1, S_1), and spectrograms (M_2, S_2). On the top part of the windows, some real-time commands are available to start/stop the acquisition, download data, record videos, or change mode settings such as PRF, downsampling factor, and CFI parameters.

equivalent performance, their implementations into a gridded layout with missing lines (see Fig. 4) impacted differently their actual performance, as already observed in [24].

The proposed architecture has been shown capable of processing the data through the MATLAB environment to continuously produce real-time B-mode images at frame rates of at least 18 Hz, depending on the configuration. Such real-time capability does not aim at a specific application but, in general, favors the experimental test of novel methods. Indeed, since research scanners are frequently used for raw data acquisition and retrospective processing, the MATLAB environment can provide, before starting the raw data acquisition, a real-time preview of the specific region under investigation. This makes the probe positioning easier during both phantom and, particularly, in-vivo experiments. The maximum frame rate could be further speeded up by improving the acquisition procedure. This currently saves files of data on the hard drive requiring several, relatively time-consuming, write/read cycles. This solution may engorge the hard drive capabilities when implementing the synchronization of several scanners. Indeed, even though modern workstations can provide tens of USB ports, a lot of files should be simultaneously transferred to and read from the hard drive. This issue could be mitigated by exploiting specific configurations of redundant array of independent disks (RAID) or by implementing a real-time data streaming towards multi-channel RAMs of the host PC. In this way, a continuous transfer rate of 100 MB/s could be sustained through the USB 3.0 link. Such throughput would, for example, permit the transfer of a 512-depth $\times$ 100-line demodulated frame in just 3.9 ms, corresponding to over 200 frames per second. Nevertheless, the optimal solution to achieve the best real-time performance, which is the ongoing work, will consist of embedding the Master-Slave modality into the

C++ real-time software. In this way, all the synchronization and the real-time processing issues would speed up by the C++ implementation, while the MATLAB environment would still be exploited as the user interface, to allow the configuration and the control of the overall system by a friendly environment.

The demonstrator was also shown capable of working according to a novel modality, in which two synchronized scanners, each associated with a distinct group of 256 elements, together transmit ultrasound beams with arbitrary shapes and independently process the received signals. A similar approach was used in [48] to implement coherent multi-transducer ultrasound imaging [49]. However, in this case, the acquisitions were started and manually saved to one distinct file for each scanner, while the real-time feedback was limited to the raw B-mode image obtained with one probe and one scanner. Here, diverging waves were simultaneously transmitted over two perpendicular planes (bi-plane imaging, Fig. 9) from a single 512-element 2-D probe (Fig. 4). In RX, the echo data received by each scanner, associated with one sub-aperture of the same probe, were beamformed over such planes. Finally, the data were processed, still in real-time, in triplex (B-mode, CFI, and MSD) mode.

It is worth highlighting that this triplex mode is highly computationally demanding as it involves high-speed parallel beamforming of 2×100 lines per TX event (i.e., at a rate of 1300 frames per second), the production of dynamic MSD profiles and high-quality HFR color flow images. Differently from the conventional line-by-line CFI, here, the HFR CFI allowed continuous-time high-pass filtering and a large packet size (32, extendable to 64) autocorrelation, while maintaining high temporal resolution (40 Hz) [41].

In conclusion, the results have shown that the synchronization of multiple ULA-OP 256, which does not require additional

hardware, could be a solution to control large matrix arrays and a valuable alternative to expensive and non-portable systems. More in general, an ultrasound architecture, with an arbitrary number of synchronous and programmable independent scanners, paves the way to a large class of applications: from the use of synchronous scanners, independently working in real-time on echo data received by different groups of elements, to the combination of multiple scanners to increase the quality of images or the processing speed during the investigations.

REFERENCES

[1] E. Boni, A. C. H. Yu, S. Freear, J. A. Jensen, and P. Tortoli, "Ultrasound open platforms for next-generation imaging technique development," *IEEE Trans. Ultrason. Ferroelect. Freq. Control*, vol. 65, no. 7, pp. 1078–1092, Jul. 2018, doi: 10.1109/TUFFC.2018.2844560.

[2] M. Tanter and M. Fink, "Ultrafast imaging in biomedical ultrasound," *IEEE Trans. Ultrason. Ferroelect. Freq. Control*, vol. 61, no. 1, pp. 102–119, Jan. 2014, doi: 10.1109/TUFFC.2014.2882.

[3] C. C. P. Cheung *et al.*, "Multi-channel pre-beamformed data acquisition system for research on advanced ultrasound imaging methods," *IEEE Trans. Ultrason. Ferroelect. Freq. Control*, vol. 59, no. 2, pp. 243–253, Feb. 2012, doi: 10.1109/TUFFC.2012.2184.

[4] J. A. Jensen, S. I. Nikolov, A. C. H. Yu, and D. Garcia, "Ultrasound vector flow imaging - Part II: Parallel systems," *IEEE Trans. Ultrason. Ferroelect. Freq. Control*, vol. 63, no. 11, pp. 1722–1732, Nov. 2016, doi: 10.1109/TUFFC.2016.2598180.

[5] E. A. Geiser, L. G. Christie, D. A. Conetta, C. R. Conti, and G. S. Gossman, "A mechanical arm for spatial registration of two-dimensional echocardiographic sections," *Catheterization Cardiovasc. Diagn.*, vol. 8, no. 1, pp. 89–101, 1982, doi: https://doi.org/10.1002/ccd.1810080114.

[6] R. Pini *et al.*, "Echocardiographic three-dimensional visualization of the heart," in *Proc. 3D Imag. Med.*, Berlin, Heidelberg, 1990, pp. 263–274, doi: 10.1007/978-3-642-84211-5_17.

[7] A. Gee, R. Prager, G. Treece, and L. Berman, "Engineering a freehand 3D ultrasound system," *Pattern Recognit. Lett.*, vol. 24, no. 4, pp. 757–777, Feb. 2003, doi: 10.1016/S0167-8655(02)00180-0.

[8] R. J. Housden, A. H. Gee, R. W. Prager, and G. M. Treece, "Rotational motion in sensorless freehand three-dimensional ultrasound," *Ultrasonics*, vol. 48, no. 5, pp. 412–422, Sep. 2008, doi: 10.1016/j.ultras.2008.01.008.

[9] T. L. A. van den Heuvel, D. J. Graham, K. J. Smith, C. L. de Korte, and J. A. Neasham, "Development of a low-cost medical ultrasound scanner using a monostatic synthetic aperture," *IEEE Trans. Biomed. Circuits Syst.*, vol. 11, no. 4, pp. 849–857, Aug. 2017, doi: 10.1109/TBCAS.2017.2695240.

[10] S. W. Smith, G. E. Trahey, and O. T. von Ramm, "Two-dimensional arrays for medical ultrasound," *Ultrason. Imag.*, vol. 14, no. 3, pp. 213–233, Jul. 1992, doi: 10.1016/0161-7346(92)90064-3.

[11] D. H. Turnbull and F. S. Foster, "Fabrication and characterization of transducer elements in two-dimensional arrays for medical ultrasound imaging," *IEEE Trans. Ultrason. Ferroelect. Freq. Control*, vol. 39, no. 4, pp. 464–475, Jul. 1992, doi: 10.1109/58.148536.

[12] R. E. Davidsen and S. W. Smith, "A two-dimensional array for B-Mode and volumetric imaging with multiplexed electrostrictive elements," *Ultrason. Imag.*, vol. 19, no. 4, pp. 235–250, Oct. 1997, doi: 10.1177/016173469701900401.

[13] B. Savord and R. Solomon, "Fully sampled matrix transducer for real time 3D ultrasonic imaging," in *Proc. 2003 IEEE Ultrason. Symp. (IUS)*, 2003, vol. 1, pp. 945–953, doi: 10.1109/ULTSYM.2003.1293556.

[14] A. Ibrahim *et al.*, "Towards ultrasound everywhere: A portable 3D digital back-end capable of zone and compound imaging," *IEEE Trans. Biomed. Circuits Syst.*, vol. 12, no. 5, pp. 968–981, Oct. 2018, doi: 10.1109/TBCAS.2018.2828342.

[15] "xMATRIX Ultrasound Technology | Philips Ultrasound, " *Philips*, (accessed on May. 2021) [Online]. Available: https://www.usa.philips.com/healthcare/resources/feature-detail/xmatrix

[16] "Vivid™ Ultra edition experience - Vivid E95." accessed on May. 2021 [Online]. Available: https://gevividultraedition.com/vivid-e95

[17] C. Chen *et al.*, "A front-end ASIC with receive Sub-array beamforming integrated with a 32 × 32 PZT matrix transducer for 3-D transesophageal echocardiography," *IEEE J. Solid-State Circuits*, vol. 52, no. 4, pp. 994–1006, Apr. 2017, doi: 10.1109/JSSC.2016.2638433.

[18] J. Janjic *et al.*, "A 2-D ultrasound transducer with front-end ASIC and low cable count for 3-D forward-looking intravascular imaging: Performance and characterization," *IEEE Trans. Ultrason. Ferroelect. Freq. Control*, vol. 65, no. 10, pp. 1832–1844, Oct. 2018, doi: 10.1109/TUFFC.2018.2859824.

[19] P. K. Weber, R. M. Schmitt, B. D. Tylkowski, and J. Steck, "Optimization of random sparse 2-D transducer arrays for 3-D electronic beam steering and focusing," in *Proc. IEEE Ultrason. Symp.*, Oct. 1994, vol. 3, pp. 1503–1506, doi: 10.1109/ULTSYM.1994.401875.

[20] G. R. Lockwood, J. R. Talman, and S. S. Brunke, "Real-time 3-D ultrasound imaging using sparse synthetic aperture beamforming," *IEEE Trans. Ultrason. Ferroelect. Freq. Control*, vol. 45, no. 4, pp. 980–988, Jul. 1998, doi: 10.1109/58.710573.

[21] A. Trucco, "Thinning and weighting of large planar arrays by simulated annealing," *IEEE Trans. Ultrason. Ferroelect. Freq. Control*, vol. 46, no. 2, pp. 347–355, Mar. 1999, doi: 10.1109/58.753023.

[22] B. Diarra, M. Robini, P. Tortoli, C. Cachard, and H. Liebgott, "Design of optimal 2-D nongrid sparse arrays for medical ultrasound," *IEEE Trans. Biomed. Eng.*, vol. 60, no. 11, pp. 3093–3102, Nov. 2013, doi: 10.1109/TBME.2013.2267742.

[23] A. Ramalli, E. Boni, A. S. Savoia, and P. Tortoli, "Density-tapered spiral arrays for ultrasound 3-D imaging," *IEEE Trans. Ultrason. Ferroelect. Freq. Control*, vol. 62, no. 8, pp. 1580–1588, Aug. 2015, doi: 10.1109/TUFFC.2015.007035.

[24] A. Ramalli *et al.*, "High-Frame-Rate tri-plane echocardiography with spiral arrays: From simulation to real-time implementation," *IEEE Trans. Ultrason. Ferroelect. Freq. Control*, vol. 67, no. 1, pp. 57–69, Jan. 2020, doi: 10.1109/TUFFC.2019.2940289.

[25] P. Mattesini, A. Ramalli, L. Petrusca, O. Basset, H. Liebgott, and P. Tortoli, "Spectral doppler measurements with 2-D sparse arrays," *IEEE Trans. Ultrason. Ferroelect. Freq. Control*, vol. 67, no. 2, pp. 278–285, Feb. 2020, doi: 10.1109/TUFFC.2019.2944090.

[26] S. Harput *et al.*, "3-D Super-Resolution ultrasound imaging with a 2-D sparse array," *IEEE Trans. Ultrason. Ferroelect. Freq. Control*, vol. 67, no. 2, pp. 269–277, Feb. 2020, doi: 10.1109/TUFFC.2019.2943646.

[27] S. Rossi, A. Ramalli, F. Fool, and P. Tortoli, "High-Frame-Rate 3-D vector flow imaging in the frequency domain," *Appl. Sci.*, vol. 10, pp. 5365, Aug. 2020, doi: 10.3390/app10155365.

[28] A. Ramalli *et al.*, "Real-time 3-D spectral doppler analysis with a sparse spiral array," *IEEE Trans. Ultrason. Ferroelect. Freq. Control*, early access, 2021, doi: 10.1109/TUFFC.2021.3051628.

[29] E. Boni *et al.*, "Architecture of an ultrasound system for continuous real-time high frame rate imaging," *IEEE Trans. Ultrason. Ferroelect. Freq. Control*, vol. 64, no. 9, pp. 1276–1284, Sep. 2017, doi: 10.1109/TUFFC.2017.2727980.

[30] J. A. Jensen *et al.*, "SARUS: A synthetic aperture real-time ultrasound system," *IEEE Trans. Ultrason. Ferroelect. Freq. Control*, vol. 60, no. 9, pp. 1838–1852, Sep. 2013, doi: 10.1109/TUFFC.2013.2770.

[31] S. Holbek *et al.*, "Ultrasonic 3-D vector flow method for quantitative in vivo peak velocity and flow rate estimation," *IEEE Trans. Ultrason. Ferroelect. Freq. Control*, vol. 64, no. 3, pp. 544–554, Mar. 2017, doi: 10.1109/TUFFC.2016.2639318.

[32] S. Holbek, T. L. Christiansen, M. B. Stuart, C. Beers, E. V. Thomsen, and J. A. Jensen, "3-D Vector flow estimation with row–column-addressed arrays," *IEEE Trans. Ultrason. Ferroelect. Freq. Control*, vol. 63, no. 11, pp. 1799–1814, Nov. 2016, doi: 10.1109/TUFFC.2016.2582536.

[33] J. Provost, C. Papadacci, C. Demene, J. Gennisson, M. Tanter, and M. Pernot, "3-D ultrafast doppler imaging applied to the noninvasive mapping of blood vessels in Vivo," *IEEE Trans. Ultrason. Ferroelect. Freq. Control*, vol. 62, no. 8, pp. 1467–1472, Aug. 2015, doi: 10.1109/TUFFC.2015.007032.

[34] L. Petrusca *et al.*, "Fast volumetric ultrasound B-Mode and doppler imaging with a new high-channels density platform for advanced 4D cardiac imaging/therapy," *Appl. Sci.*, vol. 8, no. 2, Art. no. 2, Feb. 2018, doi: 10.3390/app8020200.

[35] J. Provost *et al.*, "3D ultrafast ultrasound imaging in vivo," *Phys. Med. Biol.*, vol. 59, no. 19, pp. L1–L13, Oct. 2014, doi: 10.1088/0031-9155/59/19/L1.

[36] C. Papadacci *et al.*, "Imaging the dynamics of cardiac fiber orientation in vivo using 3D ultrasound backscatter tensor imaging," *Sci. Rep.*, vol. 7, no. 1, p. 830, Apr. 2017, doi: 10.1038/s41598-017-00946-7.

[37] E. Roux, F. Varray, L. Petrusca, C. Cachard, P. Tortoli, and H. Liebgott, "Experimental 3-D ultrasound imaging with 2-D sparse arrays using focused and diverging waves," *Sci. Rep.*, vol. 8, no. 1, p. 9108, Jun. 2018, doi: 10.1038/s41598-018-27490-2.

[38] "*us4R: a versatile research ultrasound platform*," *us4us*, (accessed Mar. 06, 2021) [Online]. Available: http://us4us.eu/product/us4r/

[39] B. Y. S. Yiu, M. Walczak, M. Lewandowski, and A. C. H. Yu, "Live ultrasound color-encoded speckle imaging platform for real-time complex flow visualization in vivo," *IEEE Trans. Ultrason. Ferroelect. Freq. Control*, vol. 66, no. 4, pp. 656–668, Apr. 2019, doi: 10.1109/TUFFC.2019.2892731.

[40] S. Ricci, L. Bassi, E. Boni, A. Dallai, and P. Tortoli, "Multi-channel FPGA-based arbitrary waveform generator for medical ultrasound," *Electron. Lett.*, vol. 43, no. 24, pp. 1335–1336, Nov. 2007, doi: 10.1049/el:20072859.

[41] F. Guidi and P. Tortoli, "Real-Time high frame rate color flow mapping system," *IEEE Trans. Ultrason. Ferroelect. Freq. Control*, pp. 1–1, 2021, doi: 10.1109/TUFFC.2021.3064612.

[42] P. Tortoli, F. Guidi, G. Guidi, and C. Atzeni, "Spectral velocity profiles for detailed ultrasound flow analysis," *IEEE Trans. Ultrason. Ferroelect. Freq. Control*, vol. 43, no. 4, pp. 654–659, Jul. 1996, doi: 10.1109/58.503727.

[43] P. Tortoli, G. Guidi, P. Berti, F. Guidi, and D. Righi, "An FFT-based flow profiler for high-resolution in vivo investigations," *Ultrasound Med. Biol.*, vol. 23, no. 6, pp. 899–910, 1997, doi: 10.1016/S0301-5629(97)00017-3.

[44] Y. Chen, L. Tong, A. Ortega, J. Luo, and J. D'hooge, "Feasibility of multiplane-transmit beamforming for real-time volumetric cardiac imaging: A simulation study," *IEEE Trans. Ultrason. Ferroelect. Freq. Control*, vol. 64, no. 4, pp. 648–659, Apr. 2017, doi: 10.1109/TUFFC.2017.2651498.

[45] C. Kasai, K. Namekawa, A. Koyano, and R. Omoto, "Real-Time two-dimensional blood flow imaging using an autocorrelation technique," *IEEE Trans. Sonics Ultrason.*, vol. 32, no. 3, pp. 458–464, May 1985, doi: 10.1109/T-SU.1985.31615.

[46] A. Ramalli *et al.*, "Real-Time high-frame-rate cardiac B-Mode and tissue doppler imaging based on multiline transmission and multiline acquisition," *IEEE Trans. Ultrason. Ferroelect. Freq. Control*, vol. 65, no. 11, pp. 2030–2041, Nov. 2018, doi: 10.1109/TUFFC.2018.2869473.

[47] K. V. Ramnarine, D. K. Nassiri, P. R. Hoskins, and J. Lubbers, "Validation of a new blood-mimicking fluid for use in doppler flow test objects," *Ultrasound Med. Biol.*, vol. 24, no. 3, pp. 451–459, Mar. 1998, doi: 10.1016/S0301-5629(97)00277-9.

[48] L. Peralta, A. Ramalli, M. Reinwald, R. J. Eckersley, and J. V. Hajnal, "Impact of aperture, depth, and acoustic clutter on the performance of coherent multi-transducer ultrasound imaging," *Appl. Sci.*, vol. 10, no. 21, Art. no. 21, Jan. 2020, doi: 10.3390/app10217655.

[49] L. Peralta, A. Gomez, Y. Luan, B.-H. Kim, J. Hajnal, and R. Eckersley, "Coherent multi-transducer ultrasound imaging," *IEEE Trans. Ultrason. Ferroelect. Freq. Control*, vol. PP, Jun. 2019, doi: 10.1109/TUFFC.2019.2921103.

Daniele Mazierli (Student Member, IEEE) received the master's degree in 2019 in electronics engineering from the University of Florence, Florence, Italy, where he is currently working toward the Ph.D. degree in information engineering.

His research interests include the design of ultrasound systems and processing algorithms for 3-D applications.

Alessandro Ramalli (Senior Member, IEEE) was born in Prato, Italy, in 1983. He received the master's degree in electronics engineering from the University of Florence, Florence, Italy, in 2008, the joint Ph.D. degree in electronics system engineering and in automation, systems and images from the University of Florence and the University of Lyon, Lyon, France, respectively, in 2012.

From 2012 to 2017, he was involved in the development of the imaging section of a programmable open ultrasound system by the University of Florence. From 2017 to 2019, he was a Postdoctoral Researcher with the Laboratory of Cardiovascular Imaging and Dynamics, KU Leuven, Leuven, Belgium, granted by the European Commission through a Marie Skłodowska-Curie Individual Fellowships, where he developed high frame rate imaging techniques for echocardiography. He is currently a Research Fellow with the University of Florence and his research interests include medical imaging, echocardiography, beamforming methods, ultrasound simulation, arrays, and systems design.

Enrico Boni (Member, IEEE) was born in 1977 in Florence, Italy. He graduated in electronic engineering from the University of Florence, Florence, Italy, in 2001 and received the Ph.D. degree in electronic system engineering from the University of Florence, in 2005.

He is currently a Researcher with Microelectronic System Design Laboratory, Department of Information Engineering, University of Florence. His research interests include analog and digital systems design, digital signal processing algorithms, digital control systems, Doppler ultrasound signal processing, microemboli detection, and classification.

Francesco Guidi (Member, IEEE) was born in Portoferraio, Italy, in 1964. He received the M.Sc. degree in electronics engineering and the Ph.D. degree in electronic systems engineering from the University of Florence, Florence, Italy.

After working with a national company, Ecs Tesak, Italy, on the design of real time radiologic image processing systems, he joined the National Institute of Nuclear Physics, where he was involved in the design of real-time software for solid-state particle detectors. Since 1992, he has been holding a position with the Information Engineering Department, University of Florence. He has authored about 100 articles in his research field, which include the development of electronic systems and real-time methods for ultrasound blood flow estimation and the investigation of acoustic properties of ultrasound contrast agents.

Piero Tortoli (Fellow, IEEE) received the Laurea degree in electronics engineering from the University of Florence, Florence, Italy, in 1978. Since then, he has been on the Faculty of the Information Engineering Department, University of Florence, where he is currently a Full Professor of electronics and was elected Member of the Academic Senate. He is leading the Microelectronics Systems Design Laboratory. He has authored more than 300 papers in his research field, which include the development of open ultrasound research systems and novel imaging or doppler methods. .

He is a Fellow of the AIMBE, Docteur Honoris causa of the University Claude Bernard Lyon 1, Villeurbanne, France, and an Honorary Member of the Polish Academy of Sciences. Since 1999, he has been on the IEEE International Ultrasonics Symposium Technical Program Committee and is currently an Associate Editor for the IEEE TRANSACTIONS ON ULTRASONICS, FERROELECTRICS, AND FREQUENCY CONTROL. He chaired the 22nd International Symposium on Acoustical Imaging in 1995, the 12th New England Doppler Conference in 2003, established the Artimino Conference on Medical Ultrasound Technology in 2011 and organized it again in 2017.